COMPUTATIONAL ANALYSIS OF SORET AND DUFOUR EFFECTS ON NANOFLUID FLOW THROUGH A STENOSED ARTERY IN THE PRESENCE OF TEMPERATURE-DEPENDENT VISCOSITY

Nidhish K. MISHRA*

*Department of Basic Science, College of Science and Theoretical Studies,
Saudi Electronic University, Riyadh 11673, Saudi Arabia

n.kumar@seu.edu.sa

received 9 December 2022, revised 18 January 2023, accepted 19 January 2023

Abstract: In this study, the Soret and Dufour effects in a composite stenosed artery were combined with an analysis of the effect of varying viscosity on copper nanofluids in a porous medium. Blood viscosity, which changes with temperature, is taken into account using the Reynolds viscosity model. The finite difference approach is used to quantitatively solve the governing equations. For use in medical applications, the effects of the physical parameters on velocity, temperature and concentration along the radial axis have been investigated and physically interpreted. The results are graphically displayed and physically defined in order to facilitate comprehension of the various phenomena that occur in the artery when nanofluid is present. It is observed that the Soret effect increases the rate of heat transfer but decreases the rate of mass transfer. The new study enhances knowledge of non-surgical treatment options for stenosis and other abnormalities, hence reducing post-operative complications. Additionally, current research may have biomedical applications such as magnetic resonance angiography (MRA), which provide a picture of an artery and enable identification of any anomalies, and thus may be useful

Keywords: Soret and Dufour effect, variable viscosity, stenosed artery, nanofluid

1. INTRODUCTION

According to the World Health Organization (WHO), about 30% of all deaths globally are caused by cardiovascular diseases (CVD), which are the leading cause of death (1). One of the main causes of health hazards is the reduced blood flow throughout our bodies as a result of artery blockages. In the circulatory system of the human body, arteries transport oxygenated blood and nutrients from the heart to each cell in the body. Red blood cells, white blood cells, platelets and plasma make up blood, a biomagnetic fluid (2). In aqueous plasma, red blood cells, white blood cells and platelets are suspended (3). Aqueous lipoproteins, nutrients and clotting factors make up plasma (4). Blood takes waste products away from the cells and assists in supplying nutrients and oxygen to the cells. The red blood cells' haemoglobin aids in the transportation of oxygen (5). Blood coagulation is aided by the platelets suspended in the plasma (6).

A frequent cause of coronary artery disease is the buildup of fatty substances inside the arterial wall lumen. Through a combination of reduced blood vessel radius and increased blood flow resistance, this process essentially limits the amount of oxygenated blood that the heart can pump to the rest of the body. Due to its critical applications in CVD such as angina, heart attacks, atherosclerosis and aneurysms, which are among the leading causes of death in the world, the haemodynamical study of stenosed arteries is an important area of research. The causes of stenosis and how it affects blood flow have been the subject of several theoretical and practical research studies. Blood travels through arteries and veins, two types of blood vessels. Based on the diameter of the arteries, blood can be classified as either a Newtonian or non-Newtonian fluid (7). Stenosis, or the accumulation of fatty materials inside the lumen, impairs blood flow in the arteries (8). The buildup of lipids in the artery wall or pathological alterations in the tissue structure cause arteriosclerosis, which affects the blood vessels (9). Heart attacks are brought on by stenosis because of increases in blood flow resistance and pressure (3). For this reason, understanding blood flow through a stenosed artery is crucial to understanding cardiovascular disorders. Blood viscosity is a crucial factor to examine because it significantly affects blood flow. Plasma viscosity and packed cell volume are the main determinants of blood viscosity (10). Viscosity is also influenced by red blood cells' mechanical characteristics. Due to their high deformability, red blood cells help the flow of blood during bulk flow and microcirculation (11). Gandhi and Sharma (12) and Poonam and Sharma (13) have examined heat and mass transfer in magnetobiofluid flow under various physical conditions.

Since there is a plethora of applications of heat and mass transfer, the effects of heat and mass transfer occurrence in porous media are receiving more attention. In this instance, the flow phenomena is more complicated than it is in a pure thermal/solutal convection process. Due to its viscosity, fluid experiences a retarding force during flow. A certain amount of energy is lost during this process. Viscous dissipation is the name given to this phenomenon. Since metallic and non-metallic nanoparticles are widely used in nano-haemodynamics, blood purification systems, nanopharmacology and the treatment of haemodynamic

disorders, it is becoming increasingly popular to study the rheological aspects of blood flow through arteries affected by cardiovascular disorders while suspending metallic or non-metallic nanoparticles. The effects of pulsing hydromagnetic flow of Au-blood non-Newtonian nanofluid in a channel in the presence of Joule heating, viscosity dissipation and thermal radiation are currently being studied by Thamizharasan and Reddy (14). Tripathi et al. (15–17) explored the interaction of magnetohydrodynamics (MHD) with a number of other important variables, including changing viscosity, Joule heating, radiation and chemical reaction. Hayat et al. (18) and Hafeez et al. (19) discussed computational analysis for velocity slip and diffusion species in the presence of magnetic field.

When heat and mass transfer occur at the same time in a moving fluid, the interactions between the fluxes and the driving potentials are more complicated. It is known that the Soret effect, which is caused by a temperature gradient, and the Dufour effect, which is caused by the concentration effect, are two different types of heat transmission. It was discovered that the Dufour effect is of a size that cannot be disregarded. Eckert and Drake (20) and Sharma et al. (21,22) analyse the thermal and mass diffusion effects on unsteady MHD free and forced convection with radiation and chemical reaction effects. Effects of Soret and Dufour on Jeffrey fluid peristaltic movement in a curved artery/channel in MHD is discussed by Hayat et al. (23). Recently, Siddique et al. (24) explore the effects of Soret and Dufour on the Casson fluid's MHD flow across a stretched surface.

In recent decades, nanofluids have been recognised as an important advancement in biomedical engineering. Theoretical and practical investigations into the potential applications of nanoparticles in blood flow problems have had a significant impact on current bioscience literature. Nanoparticles have a variety of uses, such as surgical tools for treating hyperthermia, medicine carriers, MRI, tracking agents and gene therapy. Microelectronics, fuel cells, pharmaceutical procedures, hybrid-powered engines, household refrigerators, chillers, nuclear reactor coolants, grinding and space technologies are just a few of the many heat transfer uses for nanofluids (25). Nanoparticle suspension in a base fluid is known as a nanofluid. Metals, oxides, carbides, nitrites and nanotubes are among the nanoparticles utilised in the nanofluid (26). Water, ethylene glycol, oil, biofluids and polymer solutions are the most often utilised base fluids (27). Arteriovenous stenosis is treated with nanofluids. Thermophysical characteristics such as thermal conductivity, viscosity of fluid, thermal diffusivity and convective heat transfer are improved in nanofluids (28). Gandhi et al. (29) have recently described the drug delivery applications of magnetohybrid nanoparticles (Au-Al2O3/blood) through different shape-occluded arteries by considering the viscous dissipation effect, Joule heating and variable viscosity of the fluid. As a result, monitoring blood flow while a nanofluid is present is crucial to the healing process. Some more researchers (30–34) developed mathematical models to illustrate the effect of different nanoparticles on fluid flow through different geometries.

The flow system used in all of the aforementioned research is for a fluid with constant viscosity. The viscosity of the substance might, however, differ significantly. It is vital to consider a viscosity fluctuation in order to correctly forecast flow behaviour. Hematocrit and temperature have an impact on blood viscosity, cerebral blood flow adaptation to oxygen metabolism in the brain, or both, which can affect how quickly blood flows through the brain. Blood viscosity can alter as a result of hematocrit changes. When blood temperature drops, blood viscosity rises. As temperature is lowered from 37°C to 22°C, blood viscosity rises by 50%–300% (35,36). When deliberately inducing profound hypothermia for cardiac or thoracic aortic procedures requiring temporary circulatory arrest, blood temperatures as low as 8–12°C are frequently measured (37–39). The impact of variable viscosity (temperature dependent) on MHD chemically reacting blood flow with heat and mass transfer was examined by Sharma et al. (40). Further, a mathematical model was recently created by Sharma et al. (41) to show how temperature-dependent viscosity affects blood flow through the stretching surface.

Based on the literature review and to our knowledge, no attempt is made to examine the Soret and Dufour effects on nanofluid flow through a stenosed artery in the presence of temperature-dependent viscosity. The following are the objectives and novelty of the current study: As blood viscosity is temperature-dependenttso, so the Reynolds viscosity model is considered which states that blood viscosity varies exponentially with temperature. Soret and Dufour effects on nanofluid flow through a stenosed artery are considered. No-slip boundary condition is taken into account in this case. The velocity, concentration and temperature profiles are presented using a constant pressure gradient and a steady flow assumption. Additionally covered are the Brinkmann number, viscosity parameter and Soret and Dufour effects. These findings are explained in a way that highlights the impact of different blood flow characteristics in a sick state.

2. MATHEMATICAL FORMULATION

We consider an axisymmetric flow of blood through a composite stenosed artery in a circular tubule of finite length L, as shown in Fig. 1. The geometry of the composite stenosis in an arterial wall is described by Joshi and Srivastava (42,43) as

$$\frac{R(z)}{R_0} = \begin{cases} 1 - \frac{2\delta}{R_0 L_0}(z-d) & d < z \leq d + \frac{L_0}{2} \\ 1 + \\ 1 - \frac{\delta}{2R_0}\left(\cos\frac{2\pi}{L_0}\left(z - d \right.\right. \\ \left.\left. - \frac{L_0}{2}\right)\right) & d + \frac{L_0}{2} < z \leq d + L_0 \\ 1 & otherwise \end{cases} \tag{2.1.}$$

where *R(z)* is the radius of the artery in the obstructed region, and R_0 is the radius of normal artery. Δ, L_0 and *d*, are the height, length and location of the stenosis, respectively. β is the angle of inclination of the artery from the vertical axis.

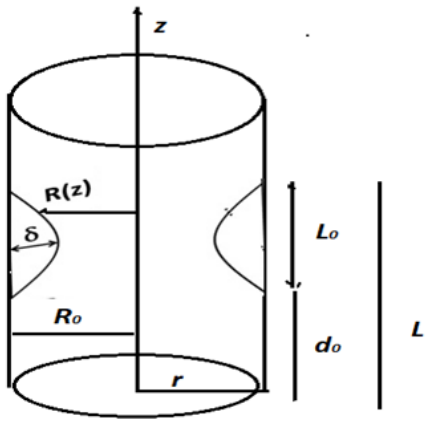

Fig. 1. Geometry of the problem

Using the above assumptions, the governing equations of the physical model can be written as the following:

Continuity equation:

$$\frac{1}{\mathrm{r}}\frac{\partial(\mathrm{rv})}{\partial \mathrm{r}}+\frac{\partial \mathrm{u}}{\partial \mathrm{z}}=0 \tag{2.2}$$

Momentum equation (r-direction):

$$\rho_{\mathrm{f}}\left(\mathrm{v}\frac{\partial \mathrm{v}}{\partial \mathrm{r}}+\mathrm{u}\frac{\partial \mathrm{v}}{\partial \mathrm{z}}\right)=-\frac{\partial \mathrm{p}}{\partial \mathrm{r}}-\left[\frac{1}{\mathrm{r}}\frac{\partial(\mathrm{r}\tau_{\mathrm{rr}})}{\partial \mathrm{r}}+\frac{\partial \tau_{\mathrm{zr}}}{\partial \mathrm{z}}-\frac{\tau_{\theta\theta}}{\mathrm{r}}\right] \tag{2.3}$$

Momentum equation (z-direction):

$$\rho_{\mathrm{f}}\left(\mathrm{v}\frac{\partial \mathrm{u}}{\partial \mathrm{r}}+\mathrm{u}\frac{\partial \mathrm{u}}{\partial \mathrm{z}}\right)=-\frac{\partial \mathrm{p}}{\partial \mathrm{z}}-\left[\frac{1}{\mathrm{r}}\frac{\partial(\mathrm{r}\tau_{\mathrm{rz}})}{\partial \mathrm{r}}+\frac{\partial \tau_{\mathrm{zz}}}{\partial \mathrm{z}}\right]$$
$$-\mu(\mathrm{T})\frac{\mathrm{u}}{\mathrm{k}_1}+\rho_{\mathrm{f}}\mathrm{g}\alpha_{\mathrm{T}}(\mathrm{T}-\mathrm{T}_0)+\rho_{\mathrm{f}}\mathrm{g}\alpha_{\mathrm{c}}(\mathrm{C}-\mathrm{C}_0) \tag{2.4}$$

Energy equation:

$$\left(\rho \mathrm{C}_{\mathrm{p}}\right)_{\mathrm{f}}\left(\mathrm{v}\frac{\partial \mathrm{T}}{\partial \mathrm{r}}+\mathrm{u}\frac{\partial \mathrm{T}}{\partial \mathrm{z}}\right)=k_T\left[\frac{\partial^2 \mathrm{T}}{\partial \mathrm{r}^2}+\frac{1}{\mathrm{r}}\frac{\partial \mathrm{T}}{\partial \mathrm{r}}+\frac{\partial^2 \mathrm{T}}{\partial \mathrm{z}^2}\right]+$$
$$\left\{\frac{\mathrm{D_m K_T}}{\mathrm{T_m}}\left[\frac{\partial^2 \mathrm{C}}{\partial \mathrm{r}^2}+\frac{1}{\mathrm{r}}\frac{\partial \mathrm{C}}{\partial \mathrm{r}}+\frac{\partial^2 \mathrm{C}}{\partial \mathrm{z}^2}\right]\right\}+\mu(\mathrm{T})\left(\frac{\partial \mathrm{u}}{\partial \mathrm{r}}\right)^2 \tag{2.5}$$

Concentration equation:

$$\left(\mathrm{v}\frac{\partial \mathrm{C}}{\partial \mathrm{r}}+\mathrm{u}\frac{\partial \mathrm{C}}{\partial \mathrm{z}}\right)=\mathrm{D_m}\left[\frac{\partial^2 \mathrm{C}}{\partial \mathrm{r}^2}+\frac{1}{\mathrm{r}}\frac{\partial \mathrm{C}}{\partial \mathrm{r}}+\frac{\partial^2 \mathrm{C}}{\partial \mathrm{z}^2}\right]$$
$$+\frac{\mathrm{D_m K_T}}{\mathrm{T_m}}\left[\frac{\partial^2 \mathrm{T}}{\partial \mathrm{r}^2}+\frac{1}{\mathrm{r}}\frac{\partial \mathrm{T}}{\partial \mathrm{r}}+\frac{\partial^2 \mathrm{T}}{\partial \mathrm{z}^2}\right] \tag{2.6}$$

The legends for the symbols used in the above equations have been defined in the nomenclature section.

The corresponding boundary conditions are the symmetry at the centreline and no-slip at the walls, as indicated below:

– At r = 0,

$$\frac{\partial \mathrm{u}}{\partial \mathrm{r}}=0,\qquad \frac{\partial \mathrm{T}}{\partial \mathrm{r}}=0,\qquad \frac{\partial \mathrm{C}}{\partial \mathrm{r}}=0 \tag{2.7}$$

– At r = $R(z)/R_0$

$$\mathrm{u}=0,\qquad \mathrm{T}=\mathrm{T}_0,\qquad \mathrm{C}=\mathrm{C}_0 \tag{2.8}$$

We proceed to introduce the following non-dimensional parameters:

$$\bar{r}=\frac{r}{R_0},\quad \bar{p}=\frac{R_0^2}{UL_0\mu_f}p,\quad \bar{z}=\frac{z}{L_0},\quad \mu(\theta)=\frac{\mu(T)}{\mu_f},$$

$$D_f=\frac{D_m K_T C_0}{\mu_f T_m C_{pf} T_0},\quad \bar{R}=\frac{R}{R_0},\ K_1=\frac{k_1}{R_0}$$

$$\bar{u}=\frac{u}{U},\ E_c=\frac{U^2}{C_{pf}T_0}, Br=E_c Pr,\quad \sigma=\frac{C-C_0}{C_0},$$

$$S_c=\frac{\mu_f}{p_f D_m},\ Gr=\frac{g\alpha_T R_0^2 T_0 \rho_f}{U\mu_f},\ P_r=\frac{\mu_f c_{pf}}{k},$$

$$\bar{v}=\frac{L_0}{\delta U}v,\quad \bar{d}=\frac{d}{L_0},\quad S_r=\frac{D_m K_T \rho T_0}{\mu T_m C_0},$$

$$Cr=\frac{g\alpha_C R_0^2 C_0 \rho_f}{U\mu_f},\quad \bar{\delta}=\frac{\delta}{R_0}, \theta=\frac{T-T_0}{T_0},\quad \alpha=\frac{k}{(\rho c_p)_f}$$

Making use of these non-dimensional variables and applying the additional conditions $\epsilon=\frac{R_0}{L_0}\cong O(1)$ for the case of mild stenosis $\left(\frac{\delta}{R_0}\ll 1\right)$ (44) to Eqs (2.1)–(2.6), the governing equations in non-dimensional form after dropping the dashes can be written as follows:

$$\frac{\partial \mathrm{p}}{\partial \mathrm{r}}=0 \tag{2.9}$$

$$\frac{\partial \mathrm{p}}{\partial \mathrm{z}}=\frac{1}{\mathrm{r}}\frac{\partial}{\partial \mathrm{r}}\left(\mathrm{r}\mu(\theta)\frac{\partial \mathrm{u}}{\partial \mathrm{r}}\right)-\left(\frac{\mu(\theta)}{\mathrm{K}_1}\right)\mathrm{u}+\mathrm{Gr}\theta+\mathrm{Cr}\sigma \tag{2.10}$$

$$\left(\frac{1}{\mathrm{r}}\frac{\partial}{\partial \mathrm{r}}\left(\mathrm{r}\frac{\partial \theta}{\partial \mathrm{r}}\right)\right)+\mathrm{DfPr}\left[\frac{1}{\mathrm{r}}\frac{\partial}{\partial \mathrm{r}}\left(\mathrm{r}\frac{\partial \sigma}{\partial \mathrm{r}}\right)\right]+\mathrm{Br}\mu(\theta)\left(\frac{\partial \mathrm{u}}{\partial \mathrm{r}}\right)^2=0 \tag{2.11}$$

$$\frac{1}{\mathrm{S_c}}\left(\frac{1}{\mathrm{r}}\frac{\partial}{\partial \mathrm{r}}\left(\mathrm{r}\frac{\partial \sigma}{\partial \mathrm{r}}\right)\right)+\mathrm{S_r}\left(\frac{1}{\mathrm{r}}\frac{\partial}{\partial \mathrm{r}}\left(\mathrm{r}\frac{\partial \theta}{\partial \mathrm{r}}\right)\right)=0 \tag{2.12}$$

Reynold's model of viscosity is considered in this study, and the same is defined as follows:

$$\mu(\theta)=e^{-\omega\theta} \tag{2.13}$$

Taking the Maclaurins expansion of the exponential terms in Eq. (2.13) and considering up to two terms, we obtain $\mu(\theta)=1-\omega\theta$.

The boundary conditions of velocity, temperature and concentration in dimensionless form are the following:

– At r = 0

$$\frac{\partial \mathrm{u}}{\partial \mathrm{r}}=0,\qquad \frac{\partial \theta}{\partial \mathrm{r}}=0,\qquad \frac{\partial \sigma}{\partial \mathrm{r}}=0 \tag{2.14}$$

– At r = R(z)

$$u=0,\qquad \theta=0\qquad \sigma=0 \tag{2.15}$$

The geometry of the arterial wall in non-dimensional form will be:

$$R(z)=\begin{Bmatrix} 1-2\delta(z-d) & d<z\leq d+\frac{1}{2} \\ 1-\frac{\delta}{2}\left(1+\cos 2\pi\left(z-d-\frac{1}{2}\right)\right) & d+\frac{1}{2}<z\leq d+1 \\ 1 & otherwise \end{Bmatrix}. \tag{2.16}$$

3. NUMERICAL SOLUTION OF THE PROBLEM

The explicit finite difference approach has been used to derive numerical solutions for the non-linear dimensionless partial differential equations with corresponding boundary conditions as mentioned above. The first order forward difference scheme is the foundation for the discretisation of first order derivative terms, whereas the central difference scheme serves as the foundation for second order terms. The blood flow zone is segmented into a grid or mesh of lines in order to obtain the difference equations. At the junction of these mesh lines, known as nodes, these difference schemes' solutions are found. A tri-diagonal system of equations is made up of the finite difference equations at every internal nodal point on a certain *n*-level. Using the Thomas algorithm (45), these equations are resolved. These are the finite difference equations:

$$\left(\frac{\partial \mathrm{p}}{\partial \mathrm{z}}\right)_{\mathrm{i,j}}=\frac{(\mu_{\mathrm{i,j}})}{\mathrm{r_{i,j}}}\left(\frac{\mathrm{u_{i+1,j}}-\mathrm{u_{i,j}}}{\Delta \mathrm{r}}\right)+(\mu_{\mathrm{i,j}})\frac{\mathrm{u_{i+1,j}}-2\mathrm{u_{i,j}}+\mathrm{u_{i-1,j}}}{(\Delta \mathrm{r})^2}-$$
$$\left(\frac{(\mu_{\mathrm{i,j}})}{\mathrm{K}}\right)\mathrm{u_{i,j}}+\left(\frac{\mathrm{u_{i+1,j}}-\mathrm{u_{i,j}}}{\Delta \mathrm{r}}\right)\left(\frac{\mu_{\mathrm{i+1,j}}-\mu_{\mathrm{i,j}}}{\Delta \mathrm{r}}\right)\mathrm{Gr}\frac{\theta_{\mathrm{i+1,j}}-\theta_{\mathrm{i,j}}}{\Delta \mathrm{r}}+$$
$$\mathrm{Cr}\frac{\sigma_{\mathrm{i+1,j}}-\sigma_{\mathrm{i,j}}}{\Delta \mathrm{r}} \tag{3.1}$$

$$\left(\frac{1}{\mathrm{r_{i,j}}}\frac{\theta_{\mathrm{i+1,j}}-\theta_{\mathrm{i,j}}}{\Delta \mathrm{r}}+\frac{\theta_{\mathrm{i+1,j}}-2\theta_{\mathrm{i,j}}+\theta_{\mathrm{i-1,j}}}{(\Delta \mathrm{r})^2}\right)+\mathrm{Br}\left(\mu_{\mathrm{i,j}}\right)\left(\left(\frac{\mathrm{u_{i+1,j}}-\mathrm{u_{i,j}}}{(\Delta \mathrm{r})^2}\right)^2\right)+$$
$$\mathrm{D_f Pr}\left(\frac{1}{\mathrm{r_{i,j}}}\frac{\sigma_{\mathrm{i+1,j}}-\sigma_{\mathrm{i,j}}}{\Delta \mathrm{r}}+\frac{\sigma_{\mathrm{i+1,j}}-2\sigma_{\mathrm{i,j}}+\sigma_{\mathrm{i-1,j}}}{(\Delta \mathrm{r})^2}\right)=0 \tag{3.2}$$

$$\frac{1}{S_c}\left(\frac{1}{r_{i,j}}\frac{\sigma_{i+1,j}-\sigma_{i,j}}{\Delta r}+\frac{\sigma_{i+1,j}-2\sigma_{i,j}+\sigma_{i-1,j}}{(\Delta r)^2}\right)+S_r\left(\frac{1}{r_{i,j}}\frac{\theta_{i+1,j}-\theta_{i,j}}{\Delta r}+\frac{\theta_{i+1,j}-2\theta_{i,j}+\theta_{i-1,j}}{(\Delta r)^2}\right)=0 \quad (3.3)$$

The appropriate mesh size for the above calculation is $\Delta r = 0.0625$. The procedure was carried out iteratively till the error was $<10^{-5}$. In order to ensure the accuracy of our results, the computation is carried out for slightly changed values of Δr. After each cycle of iteration in which the convergence criteria are assessed to confirm their validity, the values of velocity, temperature and concentration are taken note of, and on studying these values, we observe negligible change.

4. RESULTS AND DISCUSSION

The influence of the Soret and Dufour effects with permeable arterial wall and temperature-dependent viscosity, on MHD blood flow through a stenosed artery with heat and mass transfer, has been examined in this paper. Gr = 0.5, Cr = 0.3, Br = 0.3, Sc = 0.5, Sr = 0.5, Pr = 0.7, =0.02, Df*Sr = 0.12 and d = 0.25, are the default parameter values used in the calculations (46–51). Numerous numerical estimates have been made for various Sr, Df, Sc, Pr, Cr, Gr and Br values. By keeping the mean temperature *Tm* constant, the values of the Soret and Dufour numbers are selected in a way that ensures their product remains constant. Figs. 2–7 show the numerical outcomes for the velocity, temperature, concentration and shear stress profiles for various parameters. In Fig. 2, the viscosity reduces as the velocity increases. Fig. 3 depicts that with increasing the values of Sc, velocity increases. This is consistent with the physical behaviour that shows that as copper's volume percentage rises, thermal conductivity rises as well, leading to an increase in thermal boundary-layer thickness. Fig. 4 depicts the velocity curve for various values of Gr. It has been found that velocity grows as Gr increases. This is because the buoyant force is increasing as a result of the geographical variation in fluid density brought on by widening temperature differences. Additionally, as shown in Fig. 5, velocity falls as the adjusted Grashof number rises. As illustrated in Fig. 6, velocity rises as the Brinkman number rises due to an increase in heat conduction. Fig. 7 shows that blood velocity increases as the parameter K1 is raised.

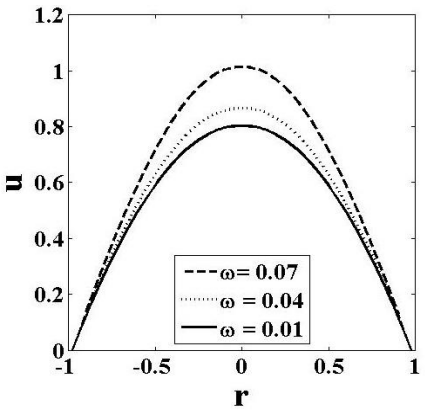

Fig. 2. Velocity profile against radial axis for varying ω

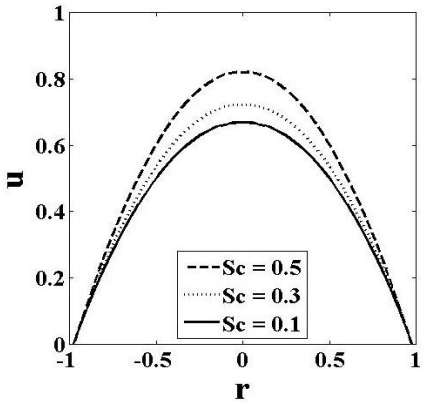

Fig. 3. Velocity profile against radial axis for varying Sc

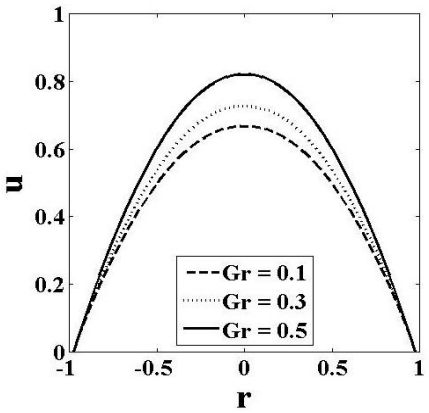

Fig. 4. Velocity profile against radial axis for varying Gr

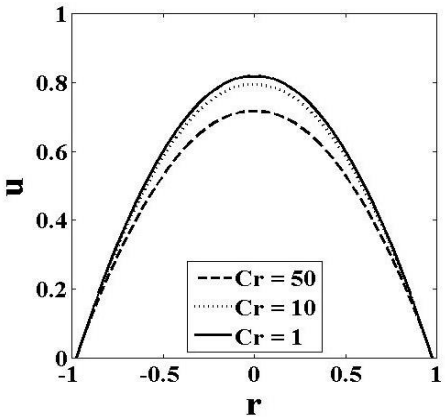

Fig. 5. Velocity profile against radial axis for varying Cr

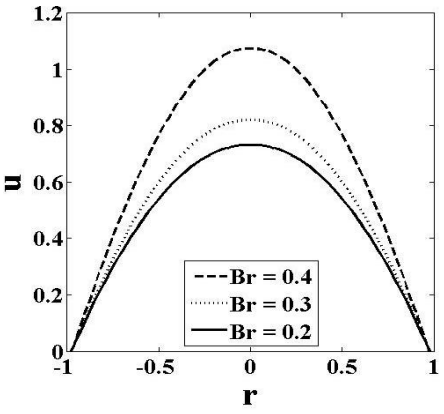

Fig. 6. Velocity profile against radial axis for varying Br

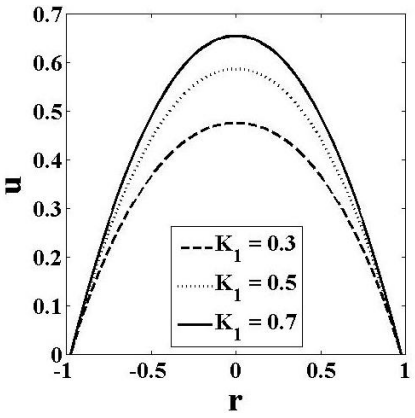

Fig. 7. Velocity profile against radial axis for varying $K1$

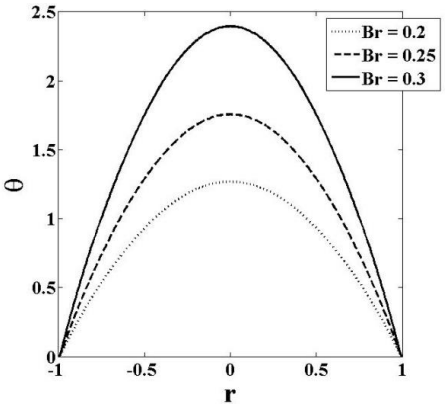

Fig. 8. Temperature profile against radial axis for varying Br

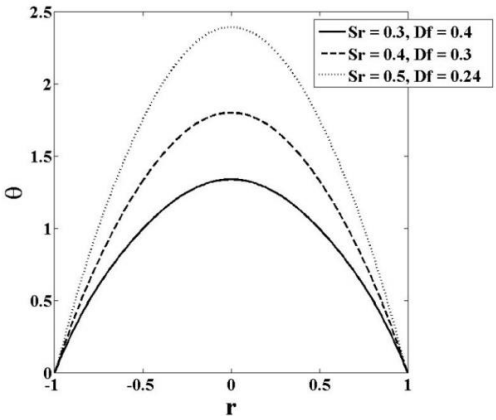

Fig. 9. Temperature profile against radial axis for varying $Sr - Df$

Temperature profiles for different values of Sr, Df, ω and Br are shown in Figs. 8–10. The influence of the Brinkman number on temperature distribution is depicted in Fig. 8. The Brinkman number measures the relationship/ratio prevailing between the heat produced by viscous dissipation and that by molecular transport.. As can be seen from Fig. 8, temperature rises as Br increases, suggesting that the viscous dissipation effect predominates over thermal diffusion in terms of temperature variation. As seen in Fig. 9, temperature rises with increasing Soret number and falls with increasing Dufour number. Owing to the temperature gradient, temperature rises as the Soret number of thermophoretic diffusion rises. Additionally, it has been found that temperature drops as the Dufour number rises because a decrease in concentration gradient results in a reduction in energy flux. As seen in Fig. 10, it is further found that temperature rises with concentration profiles for different values of ω, Sc, Sr, Df and Br are shown in Figs. 11–14.

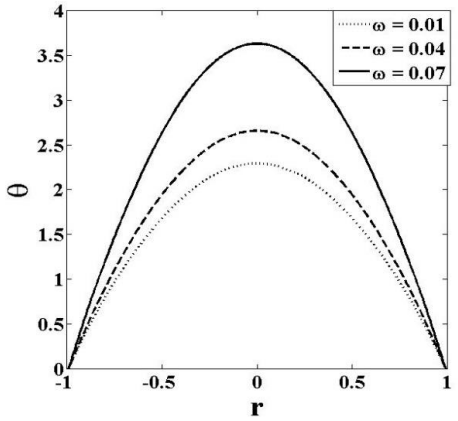

Fig. 10. Temperature profile against radial axis for varying ω

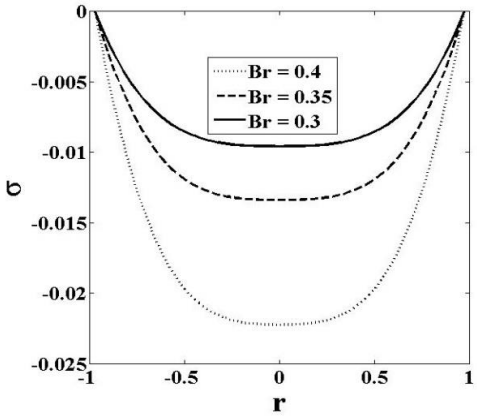

Fig. 11. Concentration profile against radial axis for varying Br

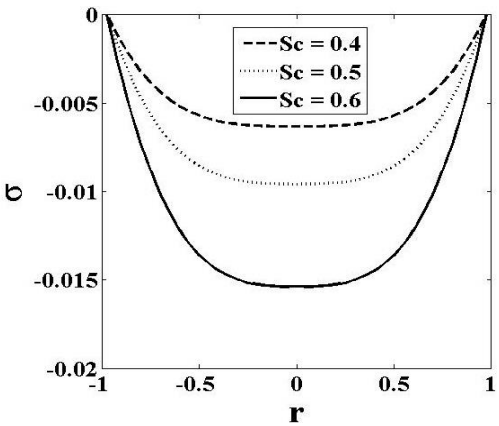

Fig. 12. Concentration profile against radial axis for varying Sc

The fluctuations of the concentration profiles of Br and Sc are depicted in Figs. 11 and 12. Additionally, it has been noted that the concentration profile behaves differently from the temperature profile. It is observed that concentration falls as the Brinkman number rises. This happens as a result of the rise in energy flux brought on by viscous dissipation. According to Fig. 12, the rise in momentum diffusivity causes concentration to fall as Sc increas-

es. As a result, the concentration buoyancy effects lessen, which lowers the fluid velocity. The thickness of the momentum and concentration boundary layers simultaneously decreases with the drops in the velocity, temperature and concentration profiles. Fig. 13 depicts the influence of Soret and Dufour numbers on the concentration field. We observe that the concentration profile descends in concatenation with the increase in the Soret number and the decrease in the Dufour number, which is attributable the fact that the gradient of concentration has gotten steeper in pursuance of the change. The influence of the viscosity parameter is shown in Fig. 14; as the viscosity parameter increases, the concentration also increases.

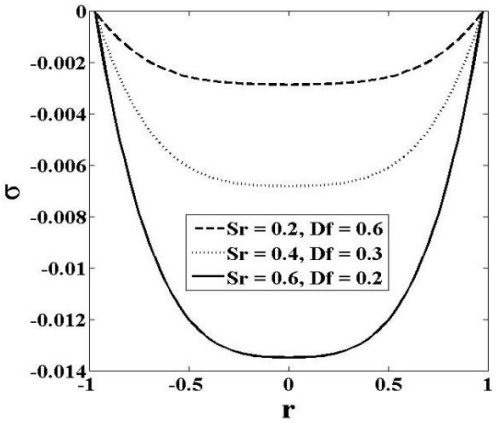

Fig. 13. Concentration profile against radial axis for varying $\mathrm{Sr} - \mathrm{Df}$

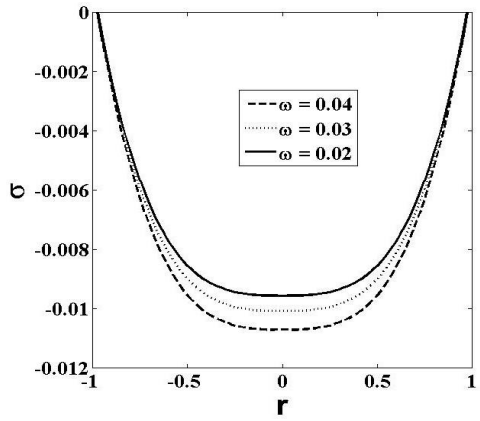

Fig. 14. Concentration profile against radial axis for varying ω

5. CONCLUSIONS

To analyse the problem of unsteady boundary layer, as well as the heat and mass transfer flow of a viscous incompressible electrically-conducting fluid (blood) through a porous medium over a composite stenosed artery subject to the Soret and Dufour effects, the finite difference method is used to solve the governing highly non-linear partial differential equations, along with the boundary conditions. The dependence of blood viscosity on temperature is taken into consideration. The key points of the above analysis are as follows:

- It is seen that velocity field rises with increasing Br, Gr, Sc and ω, whereas it decreases with increasing Cr.
- It is also noted that a reverse phenomenon is demonstrated in the concentration profile in comparison with the temperature profile.
- It is observed that increase in Br and ω increases the temperature whereas increase in Df and Pr decreases the temperature.
- The Soret number has a positive impact on the rate of heat transfer but a negative impact on the rate of mass transfer.

In addition to its utility in examining more complex difficulties involving the Soret and Dufour effects, it is envisaged that the current work will be helpful in the study of arterial blood flow issues, which can serve as the foundation for numerous scientific and industrial applications.

REFERENCES

1. Chan BT, Lim E, Chee KH, Osman NAA. Review on CFD simulation in heart with dilated cardiomyopathy and myocardial infarction. Comput Biol Med. 2013;43(4):377–385. https://doi.org/10.1016/j.compbiomed.2013.01.013. Epub 2013
2. Akbar NS, Nadeem S. Blood flow analysis in tapered stenosed arteries with pseudoplastic characteristics. Int J Biomath. 2014;7(6):1450065. https://doi.org/10.1142/S179352451450065X
3. Sankar DS. Two-phase non-linear model for blood flow in asymmetric and axisymmetric stenosed arteries. Int J Non Linear Mech. 2011;46(1):296–305. https://doi.org/10.1016/j.ijnonlinmec.2010.09.011
4. Thurston GB. Erythrocyte rigidity as a factor in blood rheology: viscoelastic dilatancy. J Rheol (N Y N Y). 1979;23(6):703–719. https://doi.org/10.1122/1.549506
5. Wolberg AS, Campbell RA. Thrombin generation, fibrin clot formation and hemostasis. Transfus Apher Sci. 2008;38(1):15–23. https://doi.org/10.1016/j.transci.2007.12.005
6. Roustaei M, Nikmaneshi MR, Firoozabadi B. Simulation of Low Density Lipoprotein (LDL) permeation into multilayer coronary arterial wall: Interactive effects of wall shear stress and fluid-structure interaction in hypertension. J Biomech. 2018;67(4):114–122.
7. Huckabe CE, Hahn AW. A generalized approach to the modeling of arterial blood flow. Bull Math Biophys. 1968;30(4):645–662. https://doi.org/10.1007/BF02476681
8. Ellahi R, Rahman SU, Nadeem S, Akbar NS. Blood flow of nanofluid through an artery with composite stenosis and permeable walls. Appl Nanosci. 2014;4(8):919–926. https://doi.org/10.1007/s13204-013-0253-6
9. Liepsch D, Singh M, Lee M. Experimental analysis of the influence of stenotic geometry on steady flow. Biorheology. 1992;29(4):419–431. https://doi.org/10.3233/bir-1992-29405
10. Lowe GD, Drummond MM, Lorimer AR, Hutton I, Forbes CD, Prentice CR, et al. Relation between extent of coronary artery disease and blood viscosity. Br Med J. 1980;280(6215):673–674. https://doi.org/ 10. 1136/bmj.280.6215.673
11. Baskurt OK, Meiselman HJ. Blood Rheology and Hemodynamics. Semin Thromb Hemost [Internet]. 2003 Nov 21 [cited 2021 Sep 11];29(05):435–450. Available from: https://doi.org/10.1055/s-2003-44551
12. Gandhi R, Sharma BK. Unsteady MHD Hybrid Nanoparticle (Au-Al 2 O 3/Blood) Mediated Blood Flow Through a Vertical Irregular Stenosed Artery: Drug Delivery Applications. In: Nonlinear Dynamics and Applications: Proceedings of the ICNDA 2022. Springer; 2022;12(2):325–337. https://doi.org/10.1007/978-3-030-99792-2_28
13. Sharma BK, Kumawat C, Vafai K. Computational biomedical simulations of hybrid nanoparticles (Au-Al2O3/blood-mediated) transport in a stenosed and aneurysmal curved artery with heat and mass transfer: Hematocrit dependent viscosity approach. Chem Phys Lett. 2022;800:139666. https://doi.org/10.1007/978-3-030-99792-2_34

14. Thamizharasan T, Reddy AS. Pulsating hydromagnetic flow of au-blood Jeffrey nanofluid in a channel with joule heating and viscous dissipation. Nanoscience and Technology: Nanosci Technol An Int J. 2022;13(2):1-13. https://doi.org/10.1615/NanoSciTechnolIntJ.2022039247
15. Tripathi B, Sharma BK, Sharma M. Modeling and analysis of MHD two-phase blood flow through a stenosed artery having temperature-dependent viscosity. Eur Phys J Plus. 2019;134(1):466. https://doi.org/10.1140/epjp/i2019-12813-9
16. Tripathi B, Sharma BK. Influence of heat and mass transfer on two-phase blood flow with joule heating and variable viscosity in the presence of variable magnetic field. Int J Comput Methods. 2020;17(03):1850139. https://doi.org/10.1142/S0219876218501396
17. Tripathi B, Sharma BK. Two-phase analysis of blood flow through a stenosed artery with the effects of chemical reaction and radiation. Ric di Mat. 2021;3(2):1-7.
18. Hayat T, Hussain Z, Alsaedi A, Hobiny A. Computational analysis for velocity slip and diffusion species with carbon nanotubes. Results Phys. 2017;7:3049–58. https://doi.org/10.1016/j.rinp.2017.07.070
19. Hafeez MB, Krawczuk M, Shahzad H. An overview of heat transfer enhancement based upon nanoparticles influenced by induced magnetic field with slip condition via finite element strategy. acta Mech Autom. 2022;16(3):200–206. https://doi.org/10.2478/ama-2022-0024
20. Eckert ERG, Drake Jr RM. Analysis of heat and mass transfer. MC Graw Hill Publishing;1974. https://doi.org/10.1016/j.rinp.2017.07.070
21. Sharma BK, Yadav K, Mishra NK, Chaudhary RC. Soret and Dufour effects on unsteady MHD mixed convection flow past a radiative vertical porous plate embedded in a porous medium with chemical reaction. 2012; 3(7):717-723. https://doi.org/ 10.4236/am.2012.37105
22. Sharma BK, Gupta S, Krishna VV, Bhargavi RJ. Soret and Dufour effects on an unsteady MHD mixed convective flow past an infinite vertical plate with Ohmic dissipation and heat source. Afrika Mat. 2014;25(3):799–821.
23. Xiao X, Wu Z-C, Chou K-C. A multi-label classifier for predicting the subcellular localization of gram-negative bacterial proteins with both single and multiple sites. PLoS One. 2011;6(6):e20592.
24. Siddique I, Nadeem M, Awrejcewicz J, Pawłowski W. Soret and Dufour effects on unsteady MHD second-grade nanofluid flow across an exponentially stretching surface. Sci Rep. 2022;12(1):11811. https://doi.org/10.1038/s41598-022-16173-8
25. Nowar K. Peristaltic flow of a nanofluid under the effect of Hall current and porous medium. Math Probl Eng. 2014;2014:1-15. https://doi.org/10.1155/2014/389581
26. Nadeem S, Ijaz S, Akbar NS. Nanoparticle analysis for blood flow of Prandtl fluid model with stenosis. Int Nano Lett. 2013;3(1):1–13. https://doi.org/10.1186/2228-5326-3-35
27. Su X, Zheng L. Hall effect on MHD flow and heat transfer of nanofluids over a stretching wedge in the presence of velocity slip and Joule heating. Cent Eur J Phys. 2013;11(12):1694–703. https://doi.org/10.2478/s11534-013-0331-0
28. Ellahi R, Rahman SU, Nadeem S. Blood flow of Jeffrey fluid in a catherized tapered artery with the suspension of nanoparticles. Phys Lett A. 2014;378(40):2973–80. https://doi.org/10.1016/j.physleta.2014.08.002
29. Ghandi R, Sharma BK, Kumawat C, Beg OA. Modeling and analysis of magnetic hybrid nanoparticle (Au-Al2O3/blood) based drug delivery through a bell-shaped occluded artery with Joule heating, viscous dissipation and variable viscosity effects. Proc Inst Mech Eng Part E J Process Mech Eng. 2022; 236(5):2024-43. https://doi.org/10.1177/09544089221080273
30. Hayat T, Hussain Z, Alsaedi A, Muhammad T. An optimal solution for magnetohydrodynamic nanofluid flow over a stretching surface with constant heat flux and zero nanoparticles flux. Neural Comput Appl. 2018;29:1555–62. https://doi.org/10.1007/s00521-016-2685-x
31. Bhandari A. Mathematical Modelling of Water-Based FeO Nanofluid Due to Rotating Disc and Comparison with Similarity Solution. acta Mech Autom. 2021;15(3):113–121. https://doi.org/10.2478/ama-2021-0016
32. Hussain Z, Hayat T, Alsaedi A, Anwar MS. Mixed convective flow of CNTs nanofluid subject to varying viscosity and reactions. Sci Rep. 2021;11(1):22838. https://doi.org/10.1038/s41598-021-02228-9
33. Hussain Z, Alshomrani AS, Muhammad T, Anwar MS. Entropy analysis in mixed convective flow of hybrid nanofluid subject to melting heat and chemical reactions. Case Stud inTherm Eng. 2022;34:101972. https://doi.org/10.1016/j.csite.2022.101972
34. Miri R, Abbassi MA, Ferhi M, Djebali R. Second Law Analysis of MHD Forced Convective Nanoliquid Flow Through a Two-Dimensional Channel. acta Mech Autom. 2022;16(4):417–431. https://doi.org/10.2478/ama-2022-0050
35. Cho HW, Hyun JM. Numerical solutions of pulsating flow and heat transfer characteristics in a pipe. Int J Heat Fluid Flow. 1990;11(4):321–330. https://doi.org/10.1016/0142-727X(90)90056-H
36. Sharma BK, Gandhi R. Combined effects of Joule heating and non-uniform heat source/sink on unsteady MHD mixed convective flow over a vertical stretching surface embedded in a Darcy-Forchheimer porous medium. Propuls Power Res. 2022;11(2):276–292. https://doi.org/10.1016/j.jppr.2022.06.001
37. Craciunescu OI, Clegg ST. Pulsatile blood flow effects on temperature distribution and heat transfer in rigid vessels. J Biomech Eng. 2001;123(5):500–505. https://doi.org/ 10.1115/1.1392318
38. Naqvi SMRS, Farooq U, Aiyashi MA, Waqas H. Comprehensive analysis of thermally radiative transport of Sisko fluid over a porous stretchable curved surface with gold nanoparticles. Int J Mod Phys B. 2022;36(03):2250028. https://doi.org/10.1142/S021797922250028X
39. Hussain Z. Heat transfer through temperature dependent viscosity hybrid nanofluid subject to homogeneous-heterogeneous reactions and melting condition: A comparative study. Phys Scr. 2020;96(1):15210. https://doi.org/10.1088/1402-4896/abc5ef
40. Sharma BK, Kumawat C, Makinde OD. Hemodynamical analysis of MHD two phase blood flow through a curved permeable artery having variable viscosity with heat and mass transfer. Biomech Model Mechanobiol. 2022;21(3):797–825. https://doi.org/10.1007/s10237-022-01561-w
41. Sharma BK, Kumawat C. Impact of temperature dependent viscosity and thermal conductivity on MHD blood flow through a stretching surface with ohmic effect and chemical reaction. Nonlinear Eng. 2021;10(1):255–271. https://doi.org/10.1515/nleng-2021-0020
42. Chakravarty S, Mandal PK. Mathematical modelling of blood flow through an overlapping arterial stenosis. Math Comput Model. 1994;19(1):59–70. https://doi.org/10.1016/0895-7177(94)90116-3
43. Chakravarty S, Mandal P. A nonlinear two-dimensional model of blood flow in an overlapping arterial stenosis subjected to body acceleration. Math Comput Model. 1996;24(1):43–58. https://doi.org/10.1016/0895-7177(96)00079-9
44. Nadeem S, Ijaz S. Theoretical analysis of metallic nanoparticles on blood flow through stenosed artery with permeable walls. Phys Lett A. 2015;379(6):542–554. https://doi.org/10.1016/j.physleta.2014.12.013
45. Datta BN. Numerical linear algebra and applications: Siam. 2010; 116. https://www.mdpi.com/journal/mathematics/special issues/ numelinear algebra
46. Sharma BK, Gandhi R, Mishra NK, Al-Mdallal QM. Entropy generation minimization of higher-order endothermic/exothermic chemical reaction with activation energy on MHD mixed convective flow over a stretching surface. Sci Rep. 2022;12(1):17688. https://doi.org/10.1038/s41598-022-22521-5
47. Sharma BK, Poonam, Chamkha AJ. Effects of heat transfer, body acceleration and hybrid nanoparticles (Au–Al2O3) on MHD blood flow through a curved artery with stenosis and aneurysm using hematocrit-dependent viscosity. Waves in Random and Complex Media. 2022;2(3):1–31. https://doi.org/10.1080/17455030.2022.2125597

48. Ali U, Irfan M, Rehman KU, Alqahtani AS, Malik MY, Shatanawi W. On the Cattaneo–Christov heat flux theory for mixed convection flow due to the rotating disk with slip effects. Waves in Random and Complex Media. 2022;4(3):1–15.
49. Sharma BK, Khanduri U, Mishra NK, Mekheimer KS. Combined effect of thermophoresis and Brownian motion on MHD mixed convective flow over an inclined stretching surface with radiation and chemical reaction. Int J Mod Phys B. 2022;2350095. https://doi.org/10.1142/S0217979223500959
50. Gandhi R, Sharma BK, Makinde OD. Entropy analysis for MHD blood flow of hybrid nanoparticles (Au–Al2O3/blood) of different shapes through an irregular stenosed permeable walled artery under periodic body acceleration: Hemodynamical applications. ZAMM-Journal Appl Math Mech für Angew Math und Mech. 2022;e202100532. https://doi.org/10.1002/zamm.202100532
51. Sharma BK, Kumar A, Gandhi R, Bhatti MM. Exponential space and thermal-dependent heat source effects on electro-magneto-hydrodynamic Jeffrey fluid flow over a vertical stretching surface. Int J Mod Phys B. 2022;36(30):2250220. https://doi.org/10.1142/S0217979222502204

Nomenclature: u represents the velocity component in the z-direction, v the velocity component in the r-direction, $R(z)$ the radius of the artery in the obstructed region, R_0 the normal artery's radius, ρ_f the effective density of the nanofluid, α_T the volume expansion coefficient with temperature, α_c the volumetric expansion coefficient with concentration, C_{pf} the specific heat of the fluid at constant pressure, σ the electrical conductivity, T_m the mean fluid temperature, D_m the coefficient of mass diffusivity, the K_T the thermal-diffusion ratio, k_T the thermal conductivity of the fluid, μ the viscosity, Pr Prandtl number, Ec Eckert number, Sr Soret number, Sc Schmidt number, ω viscosity parameter, Gr Grashof number, Cr the local concentration number, Df Dufour number and Br Brinkman number.

Nidhish Kumar MISHRA: https://orcid.org/0000-0003-4502-261X